

A CATALOG OF KEPLER HABITABLE ZONE EXOPLANET CANDIDATES

STEPHEN R. KANE¹, MICHELLE L. HILL¹, JAMES F. KASTING², RAVI KUMAR KOPPARAPU³, ELISA V. QUINTANA⁴, THOMAS BARCLAY⁴, NATALIE M. BATALHA⁴, WILLIAM J. BORUCKI⁴, DAVID R. CIARDI⁵, NADER HAGHIGHIPOUR⁶, NATALIE R. HINKEL^{1,7}, LISA KALTENEGGER⁸, FRANCK SELSIS^{9,10}, GUILLERMO TORRES¹¹

¹Department of Physics & Astronomy, San Francisco State University, 1600 Holloway Avenue, San Francisco, CA 94132, USA

²Department of Geosciences, Penn State University, 443 Deike Building, University Park, PA 16802, USA

³NASA Goddard Space Flight Center, 8800 Greenbelt Road, Mail Stop 699.0 Building 34, Greenbelt, MD 20771, USA

⁴NASA Ames Research Center, Moffett Field, CA 94035, USA

⁵NASA Exoplanet Science Institute, Caltech, MS 100-22, 770 South Wilson Avenue, Pasadena, CA 91125, USA

⁶University of Hawaii-Manoa, Honolulu, HI 96822, USA

⁷School of Earth & Space Exploration, Arizona State University, Tempe, AZ 85287, USA

⁸Department of Astronomy, Cornell University, Ithaca, NY, USA

⁹Univ. Bordeaux, LAB, UMR 5804, F-33615, Pessac, France

¹⁰CNRS, LAB, UMR 5804, F-33615, Pessac, France

¹¹Harvard-Smithsonian Center for Astrophysics, 60 Garden Street, Cambridge, MA 02138, USA

ABSTRACT

The NASA *Kepler* mission has discovered thousands of new planetary candidates, many of which have been confirmed through follow-up observations. A primary goal of the mission is to determine the occurrence rate of terrestrial-size planets within the Habitable Zone (HZ) of their host stars. Here we provide a list of HZ exoplanet candidates from the *Kepler* Data Release 24 Q1-Q17 data vetting process. This work was undertaken as part of the *Kepler* Habitable Zone Working Group. We use a variety of criteria regarding HZ boundaries and planetary sizes to produce complete lists of HZ candidates, including a catalog of 104 candidates within the optimistic HZ and 20 candidates with radii less than two Earth radii within the conservative HZ. We cross-match our HZ candidates with the Data Release 25 stellar properties and confirmed planet properties to provide robust stellar parameters and candidate dispositions. We also include false positive probabilities recently calculated by Morton (2016) for each of the candidates within our catalogs to aid in their validation. Finally, we performed dynamical analysis simulations for multi-planet systems that contain candidates with radii less than two Earth radii as a step toward validation of those systems.

Keywords: astrobiology – astronomical databases: miscellaneous – planetary systems – techniques: photometric

1. INTRODUCTION

The last few decades have seen an extraordinary progression in the field of exoplanetary science. The rate of exoplanet discovery has continued to increase as the sensitivity to smaller planets has dramatically improved. The discoveries of the *Kepler* mission have had a major impact on our understanding of exoplanet orbit, size, and multiplicity distributions (Lissauer et al. 2014; Rowe et al. 2014). The primary source of *Kepler* discoveries to the scientific community has been through the regular release and update of exoplanetary candidates (Borucki et al. 2011a,b; Batalha et al.

2013; Burke et al. 2014; Rowe et al. 2015; Mullally et al. 2015; Coughlin et al. 2016). These discoveries have shown that the frequency of planets increases to smaller sizes; thus terrestrial planets are more common than gas giant planets (Fressin et al. 2013; Howard 2013; Petigura et al. 2013).

The significance of a terrestrial-planet-rich universe is fully realized in the study of habitability. The *Kepler* mission (Borucki 2016) has a primary science goal of determining the frequency of terrestrial planets in the Habitable Zone (HZ): usually defined as the region around a star where water can exist in a liquid state on the surface of a planet with sufficient atmospheric pressure (Kasting et al. 1993). Commonly referred to as eta-Earth (η_{\oplus}), the frequency of

HZ terrestrial planets has become a major focus of interpreting *Kepler* results (Catanzarite & Shao 2011; Traub 2012; Dressing & Charbonneau 2013; Gaidos 2013; Kopparapu 2013; Foreman-Mackey et al. 2014; Morton & Swift 2014; Dressing & Charbonneau 2013). The process of determining eta-Earth requires a reliable list of HZ candidates whose properties have been adequately vetted to produce robust planetary and stellar properties.

Here we present an exhaustive catalog of HZ candidates from the Q1-Q17 Data Release 24 (DR24) candidate list, along with an analysis of the radii distributions and orbital stabilities. The work described here is the product of efforts undertaken by the *Kepler* Habitable Zone Working Group. The Q1-Q17 DR24 catalog heavily favors uniform vetting over the correct dispositions of individual objects, in order to be principally used to calculate statistically accurate occurrence rates. We cross-match the DR24 candidates with both revised stellar parameters and confirmed planets to provide the most complete list of HZ candidates from the *Kepler* mission. In Section 2 we describe the adopted boundaries for the HZ. Section 3 presents four different HZ criteria for which we present tables and statistics for candidates in each category and examine their distributions. The stability of HZ planet candidates in multi-planet systems is a necessary step in fully characterizing such planets, and we provide the results of such analyses in Section 4. Finally, we provide concluding remarks and proposals for further work in Section 5.

2. HABITABLE ZONE BOUNDARIES

The *Kepler* mission has provided several cases of confirmed planets of terrestrial size that lie in the HZ of their host star. (Borucki et al. 2012; Quintana et al. 2014; Torres et al. 2015). The concept of the HZ has appeared in the literature for some time (Huang 1959, 1960; Hart 1978, 1979), but only in recent decades have complex climate models been brought to bear on the problem of quantifying the boundaries. A key conceptual development was the inclusion of CO₂-climate feedback, introduced by Kasting et al. (1993). (Note that this feedback was also included in the Hart (1978, 1979) models, but the greenhouse effect of CO₂ was underestimated and thus he concluded that frozen planets could never deglaciate.) Importantly for our purposes, the Kasting et al. (1993) model included three sets of possible boundaries. On the inner edge, these were the moist greenhouse (in which water started to be lost), the runaway greenhouse (in which the oceans evaporate entirely), and the “recent Venus” limit (based on the empirical observation that the surface of Venus has been dry for at least a billion years). On the outer edge, the proposed limits were the “1st CO₂ condensation”

limit (where CO₂ condensation first occurs), the maximum greenhouse limit (where the CO₂ greenhouse effect maximizes), and the “early Mars” limit (based on the observation that Mars appears to have been habitable 3.8 Gyrs ago when solar luminosity was some 25% lower).

Since that time, these 1-D habitability limits have been re-evaluated using updated absorption coefficients for CO₂ and H₂O (Kopparapu et al. 2013, 2014). With the new coefficients, the moist and runaway greenhouse limits on the inner edge have coalesced. The “1st condensation” limit on the outer edge was abandoned well before this, because calculations suggested that CO₂ clouds should generally warm the climate rather than cool it (Forget & Pierrehumbert 1997; Mischna et al. 2000). This conclusion has since been revised. The early CO₂ cloud studies used two-stream approximation (Toon et al. 1989) for radiative transfer – a method that evidently overestimates the transmitted and reflected radiation, thereby yielding a higher scattering greenhouse effect (Kitzmann et al. 2013). When Kitzmann et al. (2013) used a higher-order discrete ordinate method, DISORT, with 24 radiation streams, they found a much smaller warming. Nevertheless, CO₂ clouds still do not cool a planet strongly, and so the 1st condensation limit on the outer edge can still be ignored. Now it is often considered that there are two limits at each HZ boundary, one theoretical and one empirical. The two limits for the outer edge are nearly the same, about 1.7–1.8 AU for a Sun-like star. At the inner edge, though, the theoretical runaway greenhouse limit from the Kopparapu et al. (2014) model is 0.99 AU, whereas the recent Venus limit remains at 0.75 AU (Venus itself is at 0.72 AU). The solar flux difference between the empirical and theoretical inner edges is a factor of $(0.99/0.75)^2 \cong 1.7$; thus, it makes sense to talk about a “conservative” HZ (0.99–1.7 AU) and an “optimistic” HZ (0.75–1.8 AU). Note that, as described below, the inner edge calculated by 1-D models is almost certainly overly conservative, and 0.95 AU is a better estimate for the inner HZ boundary. These limits are shown in Figure 1 as a function of the flux from the star normalized to the flux at Earth’s orbit. The boundaries vary for different stellar types because of the different albedo of an Earth-like planet under different wavelengths of stellar irradiation. HZ calculations for known exoplanet systems using these conservative and optimistic limits are available through the Habitable Zone Gallery¹ (Kane & Gelino 2012a) and described in more detail by Kane et al. (2013). A HZ calculator is also available via

¹ <http://hzgallery.org>

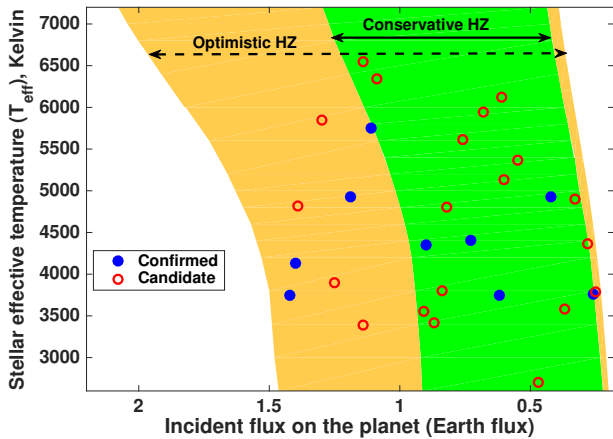


Figure 1. The stellar effective temperature as a function of incident flux for the unconfirmed candidates (open red circles) and confirmed planets (solid blue circles) from Table 2. These are overplotted on the conservative and optimistic HZ.

the website of the Virtual Planetary Laboratory².

Determining which of the HZ definitions, conservative or optimistic, is more useful depends on the task at hand. [Kasting et al. \(2014\)](#) have argued that a conservative definition should be adopted for purposes of calculating eta-Earth. That is because this parameter may eventually be used to estimate the size of a future flagship telescope mission designed to find and characterize such planets. But once such a telescope is launched and returning data, a more optimistic definition may need to be adopted in order to avoid inadvertently neglecting exoplanets that lie within the broader, empirical HZ.

Some authors have proposed modifications to the HZ limits based on additional greenhouse gases (see [Seager \(2013\)](#) for review). Specifically, accumulation of significant amounts of molecular hydrogen (H_2) in a planet's atmosphere can extend the outer edge of the HZ dramatically ([Stevenson 1999; Pierrehumbert & Gaidos 2011](#)). Molecular hydrogen condenses only at very low temperatures, and its collision-induced absorption encompasses the entire thermal-infrared spectrum ([Wordsworth & Pierrehumbert 2013](#)). [Pierrehumbert & Gaidos \(2011\)](#) showed that a 3 Earth-mass planet with 40-bar H_2 atmosphere can maintain a surface temperature of 280 K at 10 AU from a G-type star. Even free-floating terrestrial planets, with dense enough H_2 atmospheres, could remain habitable provided that they had sufficient internal heat ([Stevenson 1999](#)). But while such far flung planets may exist, it is not clear that we should allow them to influence the design of a future direct imaging telescope to observe potential habitable planets. The contrast

ratio between the Earth and the Sun is $\sim 10^{-10}$ in the visible ([Levine et al. 2006](#)), so an Earth-like planet at 10 AU, with a similar albedo, would have a contrast ratio 100 times smaller, making it difficult to observe. And free-floating habitable planets, which have an effective radiating temperature of ~ 30 K ([Stevenson 1999](#)), would be virtually impossible to detect remotely. So, it is better to accept a conservatively defined HZ for now, bearing in mind that some planets beyond this range might still be habitable.

It should also be recognized that the theoretical HZ limits are evolving with time as climate models improve. 3-D climate models can include factors such as relative humidity variations and clouds that are impossible to estimate accurately in 1-D calculations. A recent 3-D study by [Leconte et al. \(2013\)](#) shows that the inner HZ edge for a Sun-like star moves in to at least 0.95 AU because of low relative humidity in the descending branches of the tropical Hadley cells, convection cells in which air rises at the equator and sinks at medium latitudes. Another study by [Wolf & Toon \(2014\)](#) suggests that the inner edge can be even closer, at 0.93 AU, because of negative feedback from clouds. And [Yang et al. \(2013, 2014\)](#) have argued that the inner HZ edge for synchronously rotating planets around late-K and M stars could occur at a stellar flux equal to twice that at Earth's orbit because of widespread cloudiness on their sunlight sides. [Kopparapu et al. \(2016\)](#) noted that, correcting [Yang et al. \(2013, 2014\)](#) studies with consistent orbital periods, the inner edge of the HZ around M-dwarfs is further away than proposed by those studies. Nevertheless, [Kopparapu et al. \(2016\)](#) confirmed the substellar cloud mechanism originally proposed by [Yang et al. \(2013\)](#). A recent calculation by [Leconte et al. \(2015\)](#) shows that atmospheric thermal tides on M-star planets can prevent synchronous planetary rotation. Such an effect can potentially jeopardize habitability if synchronization is required to ensure a sufficient albedo, but can also favor habitability by increasing heat redistribution efficiency.

A related issue concerning the inner edge of the HZ has to do with dry planets, sometimes called “Dune” planets after the science fiction novel by that name. A (low-obliquity) Dune planet would be mostly desert but would have water-rich oases near its poles. Such planets can, in theory, remain habitable closer in to its parent star because the positive feedback caused by water vapor would be much weaker in this case. [Abe et al. \(2011\)](#) simulated such a planet with a highly parameterized 3-D climate model and determined that the inner HZ edge for a Sun-like star could be as close as 0.77 AU, near the empirical “recent Venus” limit. More recently, [Zsom et al. \(2013\)](#) approached the same problem with a 1-D climate model and determined an inner

² <http://depts.washington.edu/naivpl/content/hz-calculator>

edge of 0.38 AU. However, this result has been criticized by [Kasting et al. \(2014\)](#), who argue that a 1-D model is not appropriate for such an inherently 3-D problem, as it does not explicitly identify regions where surface liquid water might exist.

As mentioned earlier, we suggest using conservative estimates of the HZ for planet occurrence rate studies from [Kopparapu et al. \(2014\)](#). Some 3-D climate modeling studies have been used to estimate the HZ limits, but it may take time for different models to reach consensus. For this reason, in this study, we provide candidates that lie within both the conservative and optimistic estimates of the HZ from the 1-D model study of [Kopparapu et al. \(2014\)](#), which encompass the limits from 3-D models.

3. KEPLER HABITABLE ZONE CANDIDATES

We extracted the *Kepler* candidates from the NASA Exoplanet Archive³ ([Akeson et al. 2013](#)). The associated data are current as of April 26, 2016 and are derived from the Data Release 24 (DR24) table of candidates ([Coughlin et al. 2016](#)). In order to perform the necessary calculations, we required the stellar effective temperature (T_{eff}) and radius (R_{\star}), as well as the planetary parameters of semi-major axis (a) and radius (R_p). We utilize the revised stellar parameters from the Data Release 25 (DR25) stellar table ([Mathur et al. 2016](#); [Twicken et al. 2016](#)) to obtain T_{eff} and R_{\star} values, and recalculate R_p and its uncertainty using the R_p/R_{\star} values from DR24 and the R_{\star} values from DR25. Similarly, the semi-major axes are recalculated using the DR25 M_{\star} values for self-consistency. The HZ boundaries were calculated using the methodology described in Section 2 and by [Kane & Gelino \(2012a\)](#). Note that the reason cross-matching the DR24 and DR25 tables is necessary is because, although the DR25 is more recent, it only contains stellar information for the candidates. Also note that the planetary radius is not needed for the HZ calculations, but is required for the categorization process described below. We also calculate the incident flux received by the planet (F_p) in units of the solar constant:

$$\frac{F_p}{F_{\oplus}} = \left(\frac{R_{\star}}{R_{\odot}}\right)^2 \left(\frac{T_{\text{eff}}}{T_{\text{eff},\odot}}\right)^4 \left(\frac{1\text{AU}}{a}\right)^2 \quad (1)$$

The number of candidates for which we were able to extract all of the needed information for our calculations was 4,270. Those candidates for which there was insufficient information were noted by ([Coughlin et al. 2016](#)) as likely having very low signal-to-noise and are low confidence candidates.

We separate the *Kepler* candidates into four categories. Category 1 candidates are in the conservative

HZ and have a radius of $R_p < 2R_{\oplus}$. Category 2 candidates are in the optimistic HZ and have a radius of $R_p < 2R_{\oplus}$. Category 3 candidates are in the conservative HZ and can have any radius. Category 4 candidates are in the optimistic HZ and can have any radius. Clearly this means that some categories are subsets of others. For example, category 1 is a subset of category 2, and category 4 contains all of the candidates from categories 1–3. The number of exoplanet candidates in each category are 20, 29, 63, and 104 for categories 1, 2, 3, and 4 respectively. The identifiers and relevant stellar and planet parameters are shown in Tables 1, 2, 3, and 4. A handful of cases have parameter uncertainties of zero due to incomplete information in the *Kepler* data release. In cases where the candidate has been confirmed in the literature, we include the Kepler name in the second column and replace the planetary and stellar parameters with those from the relevant publications. The specific cases are Kepler-22 b ([Borucki et al. 2012](#)); Kepler-62 e & f ([Borucki et al. 2013](#)); Kepler-174 d, Kepler-283 c, Kepler-298 d, Kepler-309 c, Kepler-315 c ([Rowe et al. 2014](#)); Kepler-186 f, Kepler-440 b, Kepler-442 b, Kepler-443 b ([Torres et al. 2015](#)); Kepler-296 e & f ([Barclay et al. 2015](#)); and Kepler-452 b ([Jenkins et al. 2015](#)). The Table 2 candidates (open red circles) and confirmed planets (solid blue circles) are plotted with respect to the conservative and optimistic HZ regions in Figure 1.

Note that, even though there is a broad consensus that the boundary between terrestrial and gaseous planets likely lies close to $1.6R_{\oplus}$ ([Weiss & Marcy 2014](#); [Rogers 2015](#); [Wolfgang & Lopez 2015](#)), we use $2R_{\oplus}$ as our cut-off to account for uncertainties in the stellar and planetary parameters that would remove potentially terrestrial planets from our 1 & 2 category lists. Such a safeguard is particularly relevant in light of the fact that blended binaries may cause many of the candidate radii to be underestimated ([Cartier et al. 2015](#); [Ciardi et al. 2015](#); [Gilliland et al. 2015](#)). Recent observations of *Kepler* candidates by [Kraus et al. \(2016\)](#) revealed wide binary companions to the following candidates from Tables 1–4: K00087, K00571, K00701, K00854, K01298 K01422, K01431, K02418, K02626, K02686, K02992, K03263, K04016. The presence of a previously undetected companion can affect HZ boundaries within the system due to the additional source of stellar flux ([Kaltenegger & Haghjhipour 2012](#)), and also may impact the derived depth, and thus radius, of a planet candidate, if the flux from the newly detected companion is a significant fraction of the host star.

Determining the false positive rate (FPR) of *Kepler* candidates has been an on-going area of analysis for the past several years ([Morton & Johnson 2011](#); [Santerne et al. 2012](#); [Fressin et al. 2013](#)). Results from

³ <http://exoplanetarchive.ipac.caltech.edu>

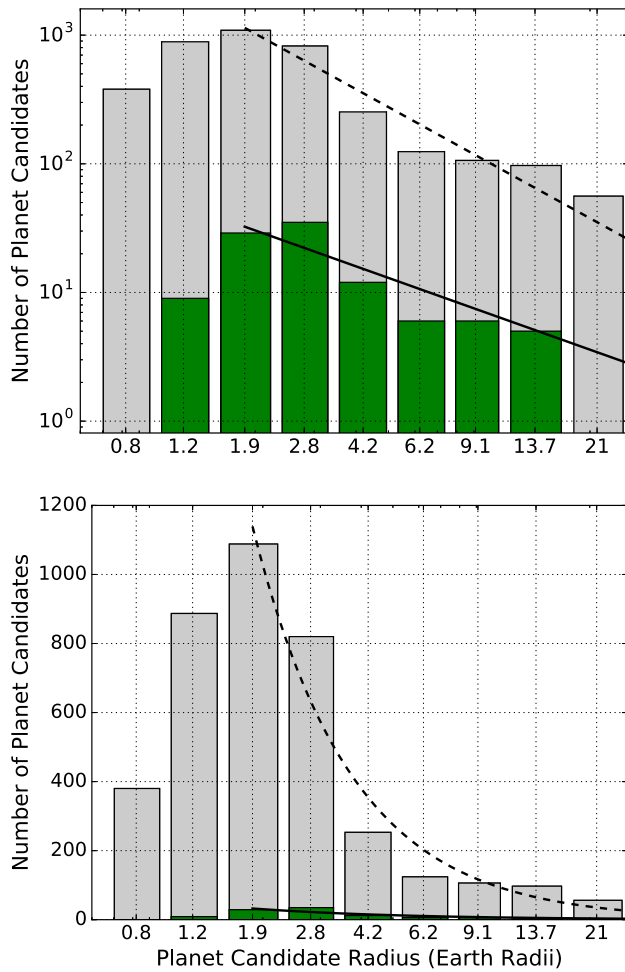


Figure 2. Histograms of all *Kepler* candidate radii (gray) relative to those candidates that are in the optimistic HZ of their host star (green), shown on a logarithmic (top panel) and linear (bottom panel) scale. The solid lines are power law fits to the HZ candidates and the dashed lines are power law fits to the entire *Kepler* distribution. Statistical analysis of the distributions shows that there is little evidence of a significant difference in the populations.

an analysis by [Désert et al. \(2015\)](#) indicate a relatively low FPR of 8.8% for *Kepler* candidates based on *Spitzer* observations and other follow-up data. For candidates with periods larger than 9–12 months, additional care must be taken to avoid false positives due to spacecraft-related systematic noise, such as artifacts on specific detector channels ([Tenenbaum et al. 2013](#); [Torres et al. 2015](#)). Manual inspection by [Coughlin et al. \(2016\)](#) found that following candidates from Tables 1–4 are likely instrumental artifacts: K06343.01, K06425.01, K07235.01, K07470.01, K07554.01, K07591.01. Recent work by [Morton \(2016\)](#) uses an automated probabilistic validation to produce false positive probabilities (FPP) for most of the *Kepler* candidates. We include these FPPs in the final column of Tables 1–4. [Morton \(2016\)](#) adopts the criteria of [Rowe et al. \(2014\)](#) that consid-

ers candidates with a FPP<1% as validated at the 99% level. Note that the automated methodology of [Morton \(2016\)](#) does not utilize follow-up observations and can calculate artificially high FPPs for candidates in multi-planet systems if dynamical interactions between the planets cause transit timing variations. Additionally, relatively large values of R_p/R_\star result in high FPP values (see for example Kepler-283 c in Table 1 with an FPP of 100%). Thus, a high FPP for a confirmed planet does not mean the confirmation is erroneous; rather it indicates that the information is insufficient to adequately determine the candidate disposition. It should further be noted that the [Morton \(2016\)](#) FPPs specifically relate to astrophysical false positives linked to transits and eclipses. As such, very low signal-to-noise candidates can actually be due to instrumental noise or stellar variability and still have low FPP values.

Shown in Figure 2 are the distribution of planet radii of all the *Kepler* candidate planets, represented by the vertical gray bars, compared with the *Kepler* candidate planets of all sizes within the optimistic HZ or their host stars (Table 4), represented by the vertical green bars. The bin edges have been set with regard to the proposed standardization of occurrence rate bins of the NASA ExoPAG Study Analysis Group 13 (private communication). The i^{th} bin in planet radius is defined as the interval $R_i = [1.5^{i-2}, 1.5^{i-1}]R_\oplus$. This implies the following bin edges (rounded to 2 significant figures and in units of R_\oplus): 0.67, 1.0, 1.5, 2.3, 3.4, 5.1, 7.6, 11, 17, 26.

We fit a power law to both distributions, represented in Figure 2 as dashed lines for all *Kepler* candidates and solid lines for the HZ candidates. The power law fits excluded the first two bins due to a lack of completeness in the data sample for planets smaller than $1.5 R_\oplus$. We use a power law of the form

$$\frac{dN}{d \log R_p} = k R_p^\alpha, \quad (2)$$

with similar notation to that used by [Howard et al. \(2012\)](#), where k and α are the power law coefficients. Note that in our case N represents the total number of planets in each radius bin. Thus, this is not intended to represent completeness but rather compare directly the radius distributions between those candidates in the HZ with those from the general *Kepler* candidate sample. The power law fits are shown in the histograms of Figure 2 where the dashed line fit uses $k = 2775$ and $\alpha = -1.44$, and the solid line fit uses $k = 57.6$ and $\alpha = -0.93$. The large difference in k is attributable to the difference in population sizes. The difference in the slope of the power laws, α , would imply that smaller planets are rarer in the HZ than in the general population. However, the transit signal of terrestrial planets

in this region is much harder to detect due to the fewer transits that occurred during the primary mission. Additionally, the orbital periods of planets in the HZ can often correspond with the rotation of the *Kepler* spacecraft over a complete solar orbit, resulting in significant systematic noise. To quantify the difference in the power laws for the two distributions, we calculated the maximum-likelihood estimator (MLE) for each sample

(Bauke 2007). For the complete sample of *Kepler* candidates, we calculate a value of $\text{MLE} = 0.68 \pm 0.01$. For the HZ candidates represented in Table 4, we calculate a value of $\text{MLE} = 0.75 \pm 0.08$. Based upon the similarity of the distributions and the MLE calculations, we conclude that there is little evidence of a significant difference in the populations.

Table 1. Category 1 HZ candidates: $R_p < 2R_\oplus$, conservative HZ

KOI Name	Kepler Name	P (days)	a (AU)	R_p (R_\oplus)	T_{eff} (K)	R_* (R_\odot)	F_p (F_\oplus)	FPP (%)
K00571.05	Kepler-186 f	129.94411 ± 0.00125	0.432	1.17 ± 0.08	3755 ± 90	0.52 ± 0.02	0.26 ± 0.04	15.840
K00701.04	Kepler-62 f	267.29099 ± 0.00500	0.718	1.41 ± 0.07	4925 ± 70	0.64 ± 0.02	0.42 ± 0.05	0.122
K01298.02	Kepler-283 c	92.74371 ± 0.00141	0.341	1.82 ± 0.12	4351 ± 100	0.57 ± 0.02	0.90 ± 0.15	100.000
K01422.04	Kepler-296 f	63.33627 ± 0.00061	0.255	1.80 ± 0.31	3740 ± 130	0.48 ± 0.08	0.62 ± 0.29	0.067
K02418.01		86.82899 ± 0.00107	0.290	1.25 ± 0.21	3576 ± 78	0.46 ± 0.05	0.37 ± 0.11	0.712
K02626.01		38.09724 ± 0.00029	0.158	1.27 ± 0.45	3554 ± 76	0.40 ± 0.05	0.91 ± 0.31	27.690
K03010.01		60.86617 ± 0.00052	0.247	1.56 ± 0.17	3808 ± 73	0.52 ± 0.03	0.84 ± 0.17	0.253
K03138.01		8.68907 ± 0.00003	0.038	0.57 ± 0.04	2703 ± 0	0.12 ± 0.00	0.47 ± 0.00	2.724
K03497.01		20.35973 ± 0.00006	0.129	0.61 ± 0.13	3419 ± 72	0.34 ± 0.06	0.87 ± 0.38	0.105
K04036.01		168.81117 ± 0.00127	0.540	1.70 ± 0.15	4798 ± 95	0.71 ± 0.03	0.82 ± 0.14	0.277
K04356.01		174.50984 ± 0.00185	0.484	1.90 ± 0.28	4367 ± 140	0.45 ± 0.05	0.28 ± 0.09	0.315
K04742.01	Kepler-442 b	112.30530 ± 0.00260	0.409	1.34 ± 0.14	4402 ± 100	0.60 ± 0.02	0.73 ± 0.11	59.110
K06343.01		569.45154 ± 0.05848	1.356	1.90 ± 0.55	6117 ± 191	0.95 ± 0.19	0.61 ± 0.32	1.048
K06425.01		521.10828 ± 0.04224	1.217	1.50 ± 0.44	5942 ± 169	0.95 ± 0.20	0.68 ± 0.36	0.481
K06676.01		439.21979 ± 0.01354	1.138	1.77 ± 0.42	6546 ± 178	0.94 ± 0.17	1.14 ± 0.53	39.220
K07223.01		317.05838 ± 0.00731	0.835	1.50 ± 0.28	5366 ± 152	0.71 ± 0.09	0.55 ± 0.19	1.802
K07235.01		299.70688 ± 0.03513	0.825	1.15 ± 0.26	5608 ± 152	0.76 ± 0.10	0.76 ± 0.29	8.719
K07470.01		392.50116 ± 0.03343	1.002	1.90 ± 0.93	5128 ± 161	0.99 ± 0.40	0.60 ± 0.56	3.805
K07554.01		482.62012 ± 0.03127	1.233	1.94 ± 0.58	6335 ± 197	1.07 ± 0.23	1.09 ± 0.61	1.306
K07591.01		328.32211 ± 0.01347	0.837	1.30 ± 0.24	4902 ± 175	0.67 ± 0.06	0.33 ± 0.11	3.146

Table 2. Category 2 HZ candidates: $R_p < 2R_\oplus$, optimistic HZ

KOI Name	Kepler Name	P (days)	a (AU)	R_p (R_\oplus)	T_{eff} (K)	R_* (R_\odot)	F_p (F_\oplus)	FPP (%)
K00463.01		18.47764 ± 0.00002	0.092	1.48 ± 0.31	3395 ± 71	0.28 ± 0.06	1.14 ± 0.54	0.005
K00571.05	Kepler-186 f	129.94411 ± 0.00125	0.432	1.17 ± 0.08	3755 ± 90	0.52 ± 0.02	0.26 ± 0.04	15.840
K00701.03	Kepler-62 e	122.38740 ± 0.00080	0.427	1.61 ± 0.05	4925 ± 70	0.64 ± 0.02	1.19 ± 0.14	0.130
K00701.04	Kepler-62 f	267.29099 ± 0.00500	0.718	1.41 ± 0.07	4925 ± 70	0.64 ± 0.02	0.42 ± 0.05	0.122
K01298.02	Kepler-283 c	92.74371 ± 0.00141	0.341	1.82 ± 0.12	4351 ± 100	0.57 ± 0.02	0.90 ± 0.15	100.000

Table 2 continued

Table 2 (*continued*)

KOI Name	Kepler Name	P (days)	a (AU)	R_p (R_{\oplus})	T_{eff} (K)	R_{\star} (R_{\odot})	F_p (F_{\oplus})	FPP (%)
K01422.04	Kepler-296 f	63.33627 ± 0.00061	0.255	1.80 ± 0.31	3740 ± 130	0.48 ± 0.08	0.62 ± 0.29	0.067
K01422.05	Kepler-296 e	34.14211 ± 0.00025	0.169	1.53 ± 0.26	3740 ± 130	0.48 ± 0.08	1.42 ± 0.67	26.410
K02418.01		86.82899 ± 0.00107	0.290	1.25 ± 0.21	3576 ± 78	0.46 ± 0.05	0.37 ± 0.11	0.712
K02626.01		38.09724 ± 0.00029	0.158	1.27 ± 0.45	3554 ± 76	0.40 ± 0.05	0.91 ± 0.31	27.690
K03010.01		60.86617 ± 0.00052	0.247	1.56 ± 0.17	3808 ± 73	0.52 ± 0.03	0.84 ± 0.17	0.253
K03138.01		8.68907 ± 0.00003	0.038	0.57 ± 0.04	2703 ± 0	0.12 ± 0.00	0.47 ± 0.00	2.724
K03282.01		49.27676 ± 0.00037	0.215	1.92 ± 0.21	3899 ± 78	0.53 ± 0.03	1.25 ± 0.26	0.065
K03497.01		20.35973 ± 0.00006	0.129	0.61 ± 0.13	3419 ± 72	0.34 ± 0.06	0.87 ± 0.38	0.105
K04036.01		168.81117 ± 0.00127	0.540	1.70 ± 0.15	4798 ± 95	0.71 ± 0.03	0.82 ± 0.14	0.277
K04087.01	Kepler-440 b	101.11141 ± 0.00078	0.242	1.86 ± 0.22	4134 ± 154	0.56 ± 0.04	1.40 ± 0.41	0.422
K04356.01		174.50984 ± 0.00185	0.484	1.90 ± 0.28	4367 ± 140	0.45 ± 0.05	0.28 ± 0.09	0.315
K04427.01		147.66022 ± 0.00146	0.419	1.68 ± 0.21	3788 ± 80	0.49 ± 0.04	0.25 ± 0.06	2.196
K04550.01		140.25252 ± 0.00215	0.465	1.95 ± 0.21	4821 ± 81	0.79 ± 0.04	1.39 ± 0.22	1.034
K04742.01	Kepler-442 b	112.30530 ± 0.00260	0.409	1.34 ± 0.14	4402 ± 100	0.60 ± 0.02	0.73 ± 0.11	59.110
K06343.01		569.45154 ± 0.05848	1.356	1.90 ± 0.55	6117 ± 191	0.95 ± 0.19	0.61 ± 0.32	1.048
K06425.01		521.10828 ± 0.04224	1.217	1.50 ± 0.44	5942 ± 169	0.95 ± 0.20	0.68 ± 0.36	0.481
K06676.01		439.21979 ± 0.01354	1.138	1.77 ± 0.42	6546 ± 178	0.94 ± 0.17	1.14 ± 0.53	39.220
K07016.01	Kepler-452 b	384.84299 ± 0.00950	1.046	1.63 ± 0.22	5757 ± 85	1.11 ± 0.12	1.11 ± 0.31	0.251
K07179.01		407.14655 ± 0.05896	1.077	1.18 ± 0.51	5845 ± 185	1.20 ± 0.30	1.30 ± 0.81	100.000
K07223.01		317.05838 ± 0.00731	0.835	1.50 ± 0.28	5366 ± 152	0.71 ± 0.09	0.55 ± 0.19	1.802
K07235.01		299.70688 ± 0.03513	0.825	1.15 ± 0.26	5608 ± 152	0.76 ± 0.10	0.76 ± 0.29	8.719
K07470.01		392.50116 ± 0.03343	1.002	1.90 ± 0.93	5128 ± 161	0.99 ± 0.40	0.60 ± 0.56	3.805
K07554.01		482.62012 ± 0.03127	1.233	1.94 ± 0.58	6335 ± 197	1.07 ± 0.23	1.09 ± 0.61	1.306
K07591.01		328.32211 ± 0.01347	0.837	1.30 ± 0.24	4902 ± 175	0.67 ± 0.06	0.33 ± 0.11	3.146

Table 3. Category 3 HZ candidates: any radius, conservative HZ

KOI Name	Kepler Name	P (days)	a (AU)	R_p (R_{\oplus})	T_{eff} (K)	R_{\star} (R_{\odot})	F_p (F_{\oplus})	FPP (%)
K00433.02		328.23996 ± 0.00036	0.917	11.24 ± 0.85	5234 ± 103	0.85 ± 0.06	0.58 ± 0.13	0.270
K00518.03	Kepler-174 d	247.35373 ± 0.00200	0.677	2.19 ± 0.13	4880 ± 126	0.62 ± 0.03	0.43 ± 0.09	0.005
K00571.05	Kepler-186 f	129.94411 ± 0.00125	0.432	1.17 ± 0.08	3755 ± 90	0.52 ± 0.02	0.26 ± 0.04	15.840
K00701.04	Kepler-62 f	267.29099 ± 0.00500	0.718	1.41 ± 0.07	4925 ± 70	0.64 ± 0.02	0.42 ± 0.05	0.122
K00841.04		269.29425 ± 0.00423	0.812	3.09 ± 0.34	5251 ± 105	0.82 ± 0.05	0.69 ± 0.15	0.161
K00854.01		56.05605 ± 0.00025	0.226	2.05 ± 0.24	3593 ± 79	0.49 ± 0.04	0.71 ± 0.18	0.005
K00868.01		235.99802 ± 0.00038	0.613	11.00 ± 0.53	4245 ± 85	0.66 ± 0.03	0.33 ± 0.05	6.834
K00881.02		226.89047 ± 0.00110	0.668	4.68 ± 0.56	5067 ± 102	0.75 ± 0.04	0.75 ± 0.14	0.240
K00902.01		83.92508 ± 0.00014	0.304	5.04 ± 0.50	3960 ± 124	0.51 ± 0.04	0.62 ± 0.18	100.000
K00959.01		12.71379 ± 0.00000	0.049	2.31 ± 0.00	2661 ± 0	0.12 ± 0.00	0.26 ± 0.00	100.000

Table 3 *continued*

Table 3 (*continued*)

KOI Name	Kepler Name	P (days)	a (AU)	R_p (R_{\oplus})	T_{eff} (K)	R_{\star} (R_{\odot})	F_p (F_{\oplus})	FPP (%)
K01126.02		475.95432 \pm 0.02806	1.037	3.05 \pm 0.61	5334 \pm 80	1.00 \pm 0.14	0.68 \pm 0.23	92.340
K01298.02	Kepler-283 c	92.74371 \pm 0.00141	0.341	1.82 \pm 0.12	4351 \pm 100	0.57 \pm 0.02	0.90 \pm 0.15	100.000
K01422.04	Kepler-296 f	63.33627 \pm 0.00061	0.255	1.80 \pm 0.31	3740 \pm 130	0.48 \pm 0.08	0.62 \pm 0.29	0.067
K01431.01		345.15988 \pm 0.00041	0.981	7.77 \pm 0.80	5597 \pm 112	0.93 \pm 0.09	0.79 \pm 0.22	78.530
K01466.01		281.56259 \pm 0.00037	0.752	11.35 \pm 0.60	4810 \pm 76	0.78 \pm 0.04	0.51 \pm 0.08	0.017
K02020.01		110.96546 \pm 0.00115	0.368	2.12 \pm 0.28	4441 \pm 140	0.55 \pm 0.04	0.77 \pm 0.22	0.473
K02078.02		161.51633 \pm 0.00086	0.496	2.87 \pm 0.22	4243 \pm 84	0.64 \pm 0.03	0.48 \pm 0.08	0.012
K02210.02		210.63058 \pm 0.00146	0.605	3.57 \pm 0.53	4895 \pm 78	0.76 \pm 0.04	0.81 \pm 0.13	0.046
K02418.01		86.82899 \pm 0.00107	0.290	1.25 \pm 0.21	3576 \pm 78	0.46 \pm 0.05	0.37 \pm 0.11	0.712
K02626.01		38.09724 \pm 0.00029	0.158	1.27 \pm 0.45	3554 \pm 76	0.40 \pm 0.05	0.91 \pm 0.31	27.690
K02686.01		211.03387 \pm 0.00083	0.611	3.83 \pm 0.38	4658 \pm 93	0.69 \pm 0.03	0.53 \pm 0.09	14.822
K02703.01		213.25766 \pm 0.00105	0.609	2.85 \pm 0.33	4477 \pm 159	0.64 \pm 0.05	0.40 \pm 0.12	0.040
K02762.01		132.99683 \pm 0.00092	0.452	2.71 \pm 0.58	4523 \pm 161	0.66 \pm 0.05	0.80 \pm 0.25	0.003
K02770.01		205.38445 \pm 0.00184	0.588	2.28 \pm 0.27	4400 \pm 157	0.62 \pm 0.05	0.38 \pm 0.12	0.789
K02834.01		136.20563 \pm 0.00128	0.460	2.39 \pm 0.31	4648 \pm 167	0.68 \pm 0.06	0.90 \pm 0.28	0.169
K02992.01		82.66049 \pm 0.00071	0.309	3.36 \pm 0.98	3952 \pm 90	0.55 \pm 0.04	0.70 \pm 0.18	80.400
K03010.01		60.86617 \pm 0.00052	0.247	1.56 \pm 0.17	3808 \pm 73	0.52 \pm 0.03	0.84 \pm 0.17	0.253
K03138.01		8.68907 \pm 0.00003	0.038	0.57 \pm 0.04	2703 \pm 0	0.12 \pm 0.00	0.47 \pm 0.00	2.724
K03263.01		76.87935 \pm 0.00005	0.262	7.90 \pm 1.77	3638 \pm 76	0.44 \pm 0.05	0.43 \pm 0.13	75.070
K03497.01		20.35973 \pm 0.00006	0.129	0.61 \pm 0.13	3419 \pm 72	0.34 \pm 0.06	0.87 \pm 0.38	0.105
K04036.01		168.81117 \pm 0.00127	0.540	1.70 \pm 0.15	4798 \pm 95	0.71 \pm 0.03	0.82 \pm 0.14	0.277
K04356.01		174.50984 \pm 0.00185	0.484	1.90 \pm 0.28	4367 \pm 140	0.45 \pm 0.05	0.28 \pm 0.09	0.315
K04385.02		386.37054 \pm 0.00859	1.014	3.17 \pm 0.34	5119 \pm 82	0.83 \pm 0.05	0.42 \pm 0.08	0.317
K04458.01		358.81808 \pm 0.00282	0.957	2.47 \pm 0.63	6056 \pm 172	0.92 \pm 0.17	1.11 \pm 0.55	42.920
K04742.01	Kepler-442 b	112.30530 \pm 0.00260	0.409	1.34 \pm 0.14	4402 \pm 100	0.60 \pm 0.02	0.73 \pm 0.11	59.110
K04745.01	Kepler-443 b	177.66930 \pm 0.00305	0.495	2.33 \pm 0.20	4723 \pm 100	0.71 \pm 0.03	0.92 \pm 0.14	0.155
K05202.01		535.93726 \pm 0.02765	1.311	2.52 \pm 0.69	5596 \pm 80	1.32 \pm 0.25	0.89 \pm 0.39	0.364
K05236.01		550.85986 \pm 0.00821	1.355	2.14 \pm 0.36	5912 \pm 77	1.12 \pm 0.15	0.74 \pm 0.23	4.900
K05276.01		220.71936 \pm 0.00558	0.651	2.20 \pm 0.37	5150 \pm 184	0.70 \pm 0.08	0.72 \pm 0.26	8.834
K05278.01		281.59155 \pm 0.00076	0.779	7.49 \pm 1.39	5330 \pm 187	0.71 \pm 0.09	0.61 \pm 0.23	0.995
K05284.01		389.31119 \pm 0.00206	1.016	6.42 \pm 2.31	5731 \pm 162	0.96 \pm 0.19	0.86 \pm 0.44	71.690
K05416.01		76.37804 \pm 0.00183	0.296	7.22 \pm 1.35	3869 \pm 140	0.58 \pm 0.06	0.78 \pm 0.26	0.103
K05622.01		469.63110 \pm 0.01246	1.112	3.23 \pm 0.75	5474 \pm 158	0.76 \pm 0.11	0.38 \pm 0.15	0.077
K05706.01		425.47784 \pm 0.01122	1.155	3.22 \pm 0.75	5977 \pm 201	1.02 \pm 0.19	0.90 \pm 0.46	0.491
K05790.01		178.26392 \pm 0.00203	0.587	3.04 \pm 0.31	4899 \pm 82	0.71 \pm 0.04	0.76 \pm 0.14	0.618
K05792.01		215.73711 \pm 0.00137	0.630	9.67 \pm 2.58	4889 \pm 175	0.72 \pm 0.07	0.68 \pm 0.23	0.618
K05850.01		303.22638 \pm 0.00246	0.878	3.62 \pm 0.64	5606 \pm 80	0.95 \pm 0.10	1.03 \pm 0.27	43.710
K05929.01		466.00378 \pm 0.00336	1.165	5.22 \pm 1.43	5830 \pm 158	0.88 \pm 0.16	0.59 \pm 0.27	29.470
K06295.01		204.26801 \pm 0.00857	0.613	11.61 \pm 1.49	4907 \pm 139	0.73 \pm 0.07	0.73 \pm 0.21	100.000
K06343.01		569.45154 \pm 0.05848	1.356	1.90 \pm 0.55	6117 \pm 191	0.95 \pm 0.19	0.61 \pm 0.32	1.048
K06384.01		566.28174 \pm 0.03469	1.285	2.78 \pm 0.66	5830 \pm 195	0.80 \pm 0.13	0.40 \pm 0.19	43.340
K06425.01		521.10828 \pm 0.04224	1.217	1.50 \pm 0.44	5942 \pm 169	0.95 \pm 0.20	0.68 \pm 0.36	0.481

Table 3 *continued*

Table 3 (*continued*)

KOI Name	Kepler Name	P (days)	a (AU)	R_p (R_{\oplus})	T_{eff} (K)	R_{\star} (R_{\odot})	F_p (F_{\oplus})	FPP (%)
K06676.01		439.21979 \pm 0.01354	1.138	1.77 \pm 0.42	6546 \pm 178	0.94 \pm 0.17	1.14 \pm 0.53	39.220
K06734.01		498.27271 \pm 0.03229	1.245	2.20 \pm 0.52	5288 \pm 79	0.97 \pm 0.10	0.43 \pm 0.11	1.613
K06786.01		455.63330 \pm 0.01771	1.153	2.96 \pm 0.73	5883 \pm 186	0.89 \pm 0.17	0.64 \pm 0.33	0.413
K07136.01		441.17368 \pm 0.04754	1.117	2.83 \pm 0.69	5395 \pm 77	1.07 \pm 0.17	0.70 \pm 0.26	59.640
K07223.01		317.05838 \pm 0.00731	0.835	1.50 \pm 0.28	5366 \pm 152	0.71 \pm 0.09	0.55 \pm 0.19	1.802
K07235.01		299.70688 \pm 0.03513	0.825	1.15 \pm 0.26	5608 \pm 152	0.76 \pm 0.10	0.76 \pm 0.29	8.719
K07345.01		377.50262 \pm 0.00857	1.053	2.18 \pm 0.33	5751 \pm 78	0.94 \pm 0.09	0.78 \pm 0.19	1.365
K07470.01		392.50116 \pm 0.03343	1.002	1.90 \pm 0.93	5128 \pm 161	0.99 \pm 0.40	0.60 \pm 0.56	3.805
K07554.01		482.62012 \pm 0.03127	1.233	1.94 \pm 0.58	6335 \pm 197	1.07 \pm 0.23	1.09 \pm 0.61	1.306
K07587.01		366.08408 \pm 0.00582	0.984	2.19 \pm 0.53	5941 \pm 198	0.94 \pm 0.20	1.03 \pm 0.57	100.000
K07591.01		328.32211 \pm 0.01347	0.837	1.30 \pm 0.24	4902 \pm 175	0.67 \pm 0.06	0.33 \pm 0.11	3.146

Table 4. Category 4 HZ candidates: any radius, optimistic HZ

KOI Name	Kepler Name	P (days)	a (AU)	R_p (R_{\oplus})	T_{eff} (K)	R_{\star} (R_{\odot})	F_p (F_{\oplus})	FPP (%)
K00087.01	Kepler-22 b	289.86230 \pm 0.00180	0.849	2.38 \pm 0.13	5518 \pm 44	0.98 \pm 0.02	1.11 \pm 0.08	2.500
K00250.04	Kepler-26 e	46.82792 \pm 0.00017	0.220	2.41 \pm 0.15	3914 \pm 119	0.51 \pm 0.02	1.13 \pm 0.23	0.009
K00433.02		328.23996 \pm 0.00036	0.917	11.24 \pm 0.85	5234 \pm 103	0.85 \pm 0.06	0.58 \pm 0.13	0.270
K00463.01		18.47764 \pm 0.00002	0.092	1.48 \pm 0.31	3395 \pm 71	0.28 \pm 0.06	1.14 \pm 0.54	0.005
K00518.03	Kepler-174 d	247.35373 \pm 0.00200	0.677	2.19 \pm 0.13	4880 \pm 126	0.62 \pm 0.03	0.43 \pm 0.09	0.005
K00571.05	Kepler-186 f	129.94411 \pm 0.00125	0.432	1.17 \pm 0.08	3755 \pm 90	0.52 \pm 0.02	0.26 \pm 0.04	15.840
K00683.01		278.12436 \pm 0.00042	0.851	5.92 \pm 0.97	5799 \pm 110	1.05 \pm 0.13	1.55 \pm 0.50	73.950
K00701.03	Kepler-62 e	122.38740 \pm 0.00080	0.427	1.61 \pm 0.05	4925 \pm 70	0.64 \pm 0.02	1.19 \pm 0.14	0.130
K00701.04	Kepler-62 f	267.29099 \pm 0.00500	0.718	1.41 \pm 0.07	4925 \pm 70	0.64 \pm 0.02	0.42 \pm 0.05	0.122
K00841.04		269.29425 \pm 0.00423	0.812	3.09 \pm 0.34	5251 \pm 105	0.82 \pm 0.05	0.69 \pm 0.15	0.161
K00854.01		56.05605 \pm 0.00025	0.226	2.05 \pm 0.24	3593 \pm 79	0.49 \pm 0.04	0.71 \pm 0.18	0.005
K00868.01		235.99802 \pm 0.00038	0.613	11.00 \pm 0.53	4245 \pm 85	0.66 \pm 0.03	0.33 \pm 0.05	6.834
K00881.02		226.89047 \pm 0.00110	0.668	4.68 \pm 0.56	5067 \pm 102	0.75 \pm 0.04	0.75 \pm 0.14	0.240
K00902.01		83.92508 \pm 0.00014	0.304	5.04 \pm 0.50	3960 \pm 124	0.51 \pm 0.04	0.62 \pm 0.18	100.000
K00959.01		12.71379 \pm 0.00000	0.049	2.31 \pm 0.00	2661 \pm 0	0.12 \pm 0.00	0.26 \pm 0.00	100.000
K01126.02		475.95432 \pm 0.02806	1.037	3.05 \pm 0.61	5334 \pm 80	1.00 \pm 0.14	0.68 \pm 0.23	92.340
K01298.02	Kepler-283 c	92.74371 \pm 0.00141	0.341	1.82 \pm 0.12	4351 \pm 100	0.57 \pm 0.02	0.90 \pm 0.15	100.000
K01411.01		305.07635 \pm 0.00034	0.913	7.85 \pm 1.30	5716 \pm 109	1.15 \pm 0.16	1.53 \pm 0.53	8.720
K01422.04	Kepler-296 f	63.33627 \pm 0.00061	0.255	1.80 \pm 0.31	3740 \pm 130	0.48 \pm 0.08	0.62 \pm 0.29	0.067
K01422.05	Kepler-296 e	34.14211 \pm 0.00025	0.169	1.53 \pm 0.26	3740 \pm 130	0.48 \pm 0.08	1.42 \pm 0.67	26.410
K01430.03	Kepler-298 d	77.47363 \pm 0.00062	0.305	2.50 \pm 0.20	4465 \pm 100	0.58 \pm 0.03	1.29 \pm 0.25	0.025
K01431.01		345.15988 \pm 0.00041	0.981	7.77 \pm 0.80	5597 \pm 112	0.93 \pm 0.09	0.79 \pm 0.22	78.530
K01466.01		281.56259 \pm 0.00037	0.752	11.35 \pm 0.60	4810 \pm 76	0.78 \pm 0.04	0.51 \pm 0.08	0.017

Table 4 *continued*

Table 4 (*continued*)

KOI Name	Kepler Name	P (days)	a (AU)	R_p (R_{\oplus})	T_{eff} (K)	R_{\star} (R_{\odot})	F_p (F_{\oplus})	FPP (%)
K01477.01		169.49954 ± 0.00115	0.544	10.83 ± 0.95	5270 ± 79	0.79 ± 0.05	1.45 ± 0.27	12.428
K01527.01		192.66299 ± 0.00155	0.633	2.88 ± 0.36	5401 ± 107	0.88 ± 0.08	1.47 ± 0.37	3.133
K01596.02	Kepler-309 c	105.35638 ± 0.00086	0.401	2.51 ± 0.18	4713 ± 100	0.72 ± 0.04	1.43 ± 0.28	3.160
K01707.02	Kepler-315 c	265.46933 ± 0.00622	0.791	4.15 ± 0.96	5796 ± 108	1.04 ± 0.20	1.75 ± 0.80	5.535
K01830.02		198.71124 ± 0.00066	0.568	3.64 ± 0.29	5180 ± 103	0.80 ± 0.05	1.28 ± 0.26	0.042
K01871.01		92.72968 ± 0.00040	0.348	2.32 ± 0.19	4580 ± 92	0.68 ± 0.03	1.48 ± 0.27	0.018
K01876.01		82.53425 ± 0.00034	0.307	2.38 ± 0.19	4316 ± 86	0.58 ± 0.03	1.11 ± 0.19	0.072
K01986.01		148.46034 ± 0.00069	0.515	3.54 ± 0.52	5159 ± 82	0.82 ± 0.05	1.62 ± 0.29	0.833
K02020.01		110.96546 ± 0.00115	0.368	2.12 ± 0.28	4441 ± 140	0.55 ± 0.04	0.77 ± 0.22	0.473
K02078.02		161.51633 ± 0.00086	0.496	2.87 ± 0.22	4243 ± 84	0.64 ± 0.03	0.48 ± 0.08	0.012
K02102.01		187.74702 ± 0.00189	0.579	3.12 ± 0.52	5303 ± 182	0.75 ± 0.09	1.20 ± 0.45	0.042
K02210.02		210.63058 ± 0.00146	0.605	3.57 ± 0.53	4895 ± 78	0.76 ± 0.04	0.81 ± 0.13	0.046
K02418.01		86.82899 ± 0.00107	0.290	1.25 ± 0.21	3576 ± 78	0.46 ± 0.05	0.37 ± 0.11	0.712
K02626.01		38.09724 ± 0.00029	0.158	1.27 ± 0.45	3554 ± 76	0.40 ± 0.05	0.91 ± 0.31	27.690
K02686.01		211.03387 ± 0.00083	0.611	3.83 ± 0.38	4658 ± 93	0.69 ± 0.03	0.53 ± 0.09	14.822
K02691.01		97.44677 ± 0.00029	0.373	3.46 ± 0.73	4735 ± 170	0.69 ± 0.06	1.53 ± 0.49	6.116
K02703.01		213.25766 ± 0.00105	0.609	2.85 ± 0.33	4477 ± 159	0.64 ± 0.05	0.40 ± 0.12	0.040
K02757.01		234.63538 ± 0.00119	0.714	2.68 ± 0.31	5422 ± 107	0.88 ± 0.08	1.19 ± 0.30	8.112
K02762.01		132.99683 ± 0.00092	0.452	2.71 ± 0.58	4523 ± 161	0.66 ± 0.05	0.80 ± 0.25	0.003
K02770.01		205.38445 ± 0.00184	0.588	2.28 ± 0.27	4400 ± 157	0.62 ± 0.05	0.38 ± 0.12	0.789
K02834.01		136.20563 ± 0.00128	0.460	2.39 ± 0.31	4648 ± 167	0.68 ± 0.06	0.90 ± 0.28	0.169
K02841.01		159.38805 ± 0.00276	0.557	2.78 ± 0.32	5135 ± 81	0.87 ± 0.06	1.54 ± 0.31	2.286
K02882.01		75.85803 ± 0.00093	0.303	2.71 ± 0.58	4474 ± 164	0.61 ± 0.06	1.48 ± 0.49	40.990
K02992.01		82.66049 ± 0.00071	0.309	3.36 ± 0.98	3952 ± 90	0.55 ± 0.04	0.70 ± 0.18	80.400
K03010.01		60.86617 ± 0.00052	0.247	1.56 ± 0.17	3808 ± 73	0.52 ± 0.03	0.84 ± 0.17	0.253
K03086.01		174.73210 ± 0.00277	0.574	3.23 ± 0.39	5201 ± 83	0.90 ± 0.07	1.60 ± 0.35	1.100
K03138.01		8.68907 ± 0.00003	0.038	0.57 ± 0.04	2703 ± 0	0.12 ± 0.00	0.47 ± 0.00	2.724
K03263.01		76.87935 ± 0.00005	0.262	7.90 ± 1.77	3638 ± 76	0.44 ± 0.05	0.43 ± 0.13	75.070
K03282.01		49.27676 ± 0.00037	0.215	1.92 ± 0.21	3899 ± 78	0.53 ± 0.03	1.25 ± 0.26	0.065
K03497.01		20.35973 ± 0.00006	0.129	0.61 ± 0.13	3419 ± 72	0.34 ± 0.06	0.87 ± 0.38	0.105
K03663.01	Kepler-86 b	282.52548 ± 0.00011	0.845	9.13 ± 0.93	5725 ± 108	0.91 ± 0.09	1.12 ± 0.31	0.000
K03726.01		115.99435 ± 0.00005	0.419	14.69 ± 1.08	4530 ± 159	0.74 ± 0.05	1.17 ± 0.32	21.640
K03823.01		202.11754 ± 0.00034	0.667	5.79 ± 0.62	5536 ± 79	0.92 ± 0.08	1.59 ± 0.38	33.580
K04016.01		125.41312 ± 0.00042	0.420	2.69 ± 0.24	4641 ± 79	0.75 ± 0.03	1.32 ± 0.20	0.282
K04036.01		168.81117 ± 0.00127	0.540	1.70 ± 0.15	4798 ± 95	0.71 ± 0.03	0.82 ± 0.14	0.277
K04051.01		163.69235 ± 0.00138	0.563	2.87 ± 0.29	4999 ± 79	0.84 ± 0.05	1.25 ± 0.23	0.396
K04054.01		169.13345 ± 0.00140	0.569	2.04 ± 0.19	5171 ± 103	0.80 ± 0.05	1.27 ± 0.26	2.210
K04084.01		214.88655 ± 0.00311	0.696	3.08 ± 0.50	5323 ± 79	1.00 ± 0.12	1.47 ± 0.45	0.062
K04087.01	Kepler-440 b	101.11141 ± 0.00078	0.242	1.86 ± 0.22	4134 ± 154	0.56 ± 0.04	1.40 ± 0.41	0.422
K04103.01		184.77185 ± 0.00155	0.568	2.56 ± 0.25	5273 ± 105	0.80 ± 0.05	1.38 ± 0.29	0.608
K04121.01		198.08878 ± 0.00246	0.626	3.47 ± 0.53	5275 ± 83	0.97 ± 0.11	1.67 ± 0.47	0.038
K04356.01		174.50984 ± 0.00185	0.484	1.90 ± 0.28	4367 ± 140	0.45 ± 0.05	0.28 ± 0.09	0.315

Table 4 *continued*

Table 4 (*continued*)

KOI Name	Kepler Name	P (days)	a (AU)	R_p (R_{\oplus})	T_{eff} (K)	R_{\star} (R_{\odot})	F_p (F_{\oplus})	FPP (%)
K04385.02		386.37054 ± 0.00859	1.014	3.17 ± 0.34	5119 ± 82	0.83 ± 0.05	0.42 ± 0.08	0.317
K04427.01		147.66022 ± 0.00146	0.419	1.68 ± 0.21	3788 ± 80	0.49 ± 0.04	0.25 ± 0.06	2.196
K04458.01		358.81808 ± 0.00282	0.957	2.47 ± 0.63	6056 ± 172	0.92 ± 0.17	1.11 ± 0.55	42.920
K04550.01		140.25252 ± 0.00215	0.465	1.95 ± 0.21	4821 ± 81	0.79 ± 0.04	1.39 ± 0.22	1.034
K04742.01	Kepler-442 b	112.30530 ± 0.00260	0.409	1.34 ± 0.14	4402 ± 100	0.60 ± 0.02	0.73 ± 0.11	59.110
K04745.01	Kepler-443 b	177.66930 ± 0.00305	0.495	2.33 ± 0.20	4723 ± 100	0.71 ± 0.03	0.92 ± 0.14	0.155
K05202.01		535.93726 ± 0.02765	1.311	2.52 ± 0.69	5596 ± 80	1.32 ± 0.25	0.89 ± 0.39	0.364
K05236.01		550.85986 ± 0.00821	1.355	2.14 ± 0.36	5912 ± 77	1.12 ± 0.15	0.74 ± 0.23	4.900
K05276.01		220.71936 ± 0.00558	0.651	2.20 ± 0.37	5150 ± 184	0.70 ± 0.08	0.72 ± 0.26	8.834
K05278.01		281.59155 ± 0.00076	0.779	7.49 ± 1.39	5330 ± 187	0.71 ± 0.09	0.61 ± 0.23	0.995
K05284.01		389.31119 ± 0.00206	1.016	6.42 ± 2.31	5731 ± 162	0.96 ± 0.19	0.86 ± 0.44	71.690
K05416.01		76.37804 ± 0.00183	0.296	7.22 ± 1.35	3869 ± 140	0.58 ± 0.06	0.78 ± 0.26	0.103
K05475.01		448.30356 ± 0.00416	1.085	2.63 ± 0.72	6072 ± 152	1.29 ± 0.32	1.71 ± 1.02	0.715
K05552.01		295.95807 ± 0.00202	0.815	2.15 ± 0.37	5505 ± 104	0.99 ± 0.12	1.22 ± 0.40	1.840
K05581.01		374.87625 ± 0.00711	1.053	4.92 ± 2.01	5636 ± 171	1.35 ± 0.36	1.50 ± 0.97	0.275
K05622.01		469.63110 ± 0.01246	1.112	3.23 ± 0.75	5474 ± 158	0.76 ± 0.11	0.38 ± 0.15	0.077
K05706.01		425.47784 ± 0.01122	1.155	3.22 ± 0.75	5977 ± 201	1.02 ± 0.19	0.90 ± 0.46	0.491
K05790.01		178.26392 ± 0.00203	0.587	3.04 ± 0.31	4899 ± 82	0.71 ± 0.04	0.76 ± 0.14	0.618
K05792.01		215.73711 ± 0.00137	0.630	9.67 ± 2.58	4889 ± 175	0.72 ± 0.07	0.68 ± 0.23	0.618
K05850.01		303.22638 ± 0.00246	0.878	3.62 ± 0.64	5606 ± 80	0.95 ± 0.10	1.03 ± 0.27	43.710
K05929.01		466.00378 ± 0.00336	1.165	5.22 ± 1.43	5830 ± 158	0.88 ± 0.16	0.59 ± 0.27	29.470
K06295.01		204.26801 ± 0.00857	0.613	11.61 ± 1.49	4907 ± 139	0.73 ± 0.07	0.73 ± 0.21	100.000
K06343.01		569.45154 ± 0.05848	1.356	1.90 ± 0.55	6117 ± 191	0.95 ± 0.19	0.61 ± 0.32	1.048
K06384.01		566.28174 ± 0.03469	1.285	2.78 ± 0.66	5830 ± 195	0.80 ± 0.13	0.40 ± 0.19	43.340
K06425.01		521.10828 ± 0.04224	1.217	1.50 ± 0.44	5942 ± 169	0.95 ± 0.20	0.68 ± 0.36	0.481
K06676.01		439.21979 ± 0.01354	1.138	1.77 ± 0.42	6546 ± 178	0.94 ± 0.17	1.14 ± 0.53	39.220
K06734.01		498.27271 ± 0.03229	1.245	2.20 ± 0.52	5288 ± 79	0.97 ± 0.10	0.43 ± 0.11	1.613
K06786.01		455.63330 ± 0.01771	1.153	2.96 ± 0.73	5883 ± 186	0.89 ± 0.17	0.64 ± 0.33	0.413
K07016.01	Kepler-452 b	384.84299 ± 0.00950	1.046	1.63 ± 0.22	5757 ± 85	1.11 ± 0.12	1.11 ± 0.31	0.251
K07040.01		502.20642 ± 0.04742	1.152	3.61 ± 1.44	6346 ± 82	1.21 ± 0.14	1.62 ± 0.46	60.420
K07136.01		441.17368 ± 0.04754	1.117	2.83 ± 0.69	5395 ± 77	1.07 ± 0.17	0.70 ± 0.26	59.640
K07179.01		407.14655 ± 0.05896	1.077	1.18 ± 0.51	5845 ± 185	1.20 ± 0.30	1.30 ± 0.81	100.000
K07223.01		317.05838 ± 0.00731	0.835	1.50 ± 0.28	5366 ± 152	0.71 ± 0.09	0.55 ± 0.19	1.802
K07235.01		299.70688 ± 0.03513	0.825	1.15 ± 0.26	5608 ± 152	0.76 ± 0.10	0.76 ± 0.29	8.719
K07345.01		377.50262 ± 0.00857	1.053	2.18 ± 0.33	5751 ± 78	0.94 ± 0.09	0.78 ± 0.19	1.365
K07470.01		392.50116 ± 0.03343	1.002	1.90 ± 0.93	5128 ± 161	0.99 ± 0.40	0.60 ± 0.56	3.805
K07554.01		482.62012 ± 0.03127	1.233	1.94 ± 0.58	6335 ± 197	1.07 ± 0.23	1.09 ± 0.61	1.306
K07587.01		366.08408 ± 0.00582	0.984	2.19 ± 0.53	5941 ± 198	0.94 ± 0.20	1.03 ± 0.57	100.000
K07591.01		328.32211 ± 0.01347	0.837	1.30 ± 0.24	4902 ± 175	0.67 ± 0.06	0.33 ± 0.11	3.146

4. DYNAMICAL STABILITY OF HZ CANDIDATES

Of the 29 HZ candidates from category 2 (radii less than $2R_{\oplus}$ and within the optimistic HZ; Table 2), 6

are in multi-planet systems. Specifically, 3 five-planet systems (Kepler-62, Kepler-186 and Kepler-296) and 1 double system (Kepler-283c) harbor these 6 candidates. For the candidates of any radii within the optimistic HZ (Table 4), 19 are in multi-planet systems (13 double systems, 4 triple systems, and 2 quadruple system). Six of these candidates from Table 2 and four from Table 4 have been confirmed, however only a few have had a thorough dynamical stability analysis performed (Bolmont et al. 2014, 2015; Shields et al. 2016). Here we examine the orbital stability of all HZ candidates that orbit in multi-planet systems. For the small ($< 2R_{\oplus}$) candidates, we further explore long-term stability for a wide range of plausible eccentricities and compositions.

To perform stability analyses, we first need to provide masses for the planets, as transit photometry only provides planetary radii. The candidates (at least those from Table 2) are too small to induce gravitational perturbations on their star or on adjacent planets, so neither radial velocity observations nor transit timing variations can be used to constrain their masses. We therefore turn to mass-radius relations of the form

$$M_p = M_{\oplus} (R_p / R_{\oplus})^{\alpha} \quad (3)$$

where M_p and R_p are the mass and radius of the planet, respectively, and α is a model-dependent exponent. We tested for stability using several models for α that were derived theoretically (Lissauer et al. 2011; Valencia et al. 2006; Fortney et al. 2007) and empirically (Weiss & Marcy 2014) for completeness.

For two-planet systems, the criterion for stability is that their separations Δ exceed about 3.5 mutual Hill radii (R_{H,M_p}) (Gladman 1993), where

$$R_{H,M_p} = 0.5 (a_{in} + a_{out}) [(M_{p,in} + M_{p,out}) / 3M_{\star}]^{1/3} \quad (4)$$

and

$$\Delta = (a_{out} - a_{in}) / R_H \quad (5)$$

Here a is the semimajor axis, M_p is the planet mass, M_{\star} is the central mass and ‘in/out’ subscripts represent the inner and outer planets. The two-planet system from Table 2 (Kepler-283c) and all two-planet systems from Table 4 obey this constraint, with Δ values ranging from 19–116.

For systems with more than two planets, Smith & Lissauer (2009) established a heuristic criterion of $\Delta \sim 9$ between adjacent planets in order to have long-term stability on Gyr timescales. In some cases Δ can be lower if an adjacent Δ is higher, so they imposed a criterion of $\Delta_{in} + \Delta_{out} > 18$ for three adjacent planets. The five-planet systems from Table 2 (Kepler-186, Kepler-62, and Kepler-296) all satisfy these criteria, as do all multi-planet systems from Table 4.

4.1. Eccentricities

For the multi-planets systems in Table 2, we numerically explored the dynamical stability using the *Mercury* integration package (Chambers 1999) in order to examine the effect of higher eccentricities on the long-term survival of the systems. Using masses derived from the Lissauer et al. (2011) mass-radius relation, we explored stability for a full range of eccentricities assigned to the HZ candidates, simulating each case with all other planets in the system on nearly circular and coplanar orbits. Note that higher eccentricities for the candidate will likely induce, or will be a result of, planet-planet interactions, however our goal is to examine the maximum eccentricity value that could destabilize the system. We evolved each system forward in time for 10^{10} orbits of the outermost planet using a time-step of 1/20 times the orbital period of the innermost planet. Constraints (upper limits) on eccentricities from these simulations are 0.3 for both Kepler-62e and f, 0.62 for Kepler-186f, 0.72 for Kepler-283c, and 0.14 and 0.16 for Kepler-296 e and f, respectively. Note that eccentric orbits for planets within the HZ can produce seasonal variations that inhibit the consistent presence of liquid water on the surface (Williams & Pollard 2002; Kane & Gelino 2012b; Bolmont et al. 2016).

4.2. Densities

We also explored stability for a wide range of plausible compositions for the planets with radii $< 2R_{\oplus}$. By adopting a planetary composition model, an estimate of the planet mass is obtained whilst providing insight into possible interior structures. Data from the dozens of exoplanets that have both measured masses and radii (and therefore densities), combined with theoretical models, suggest that planets with radii less than about $1.6R_{\oplus}$ are likely composed of some combination of ice, silicate rock and iron and devoid of massive gaseous H/He envelopes (Rogers 2015). While the HZ candidates with radii closer to $2R_{\oplus}$ are likely H/He-rich sub-Neptunes, in theory they could still be rocky, as thermal evolution models predict a hard upper limit for the size of an envelope-free planet at about $2R_{\oplus}$ (Lopez & Fortney 2014). For our stability analysis of the candidates from Table 2, we assume the planets haven’t accreted enough gas to significantly alter their radii. Using radius-composition curves from Fortney et al. (2007), we explored the stability of these systems using compositions with different ratios of ice, rock and iron (from pure ice to pure iron). For nearly all systems, the extreme case of pure iron planets allowed long-term stability for all planets in the system. The exception is Kepler-296 in which the highest density for all planets that allowed long-term stability was a 50/50% Earth-like/iron composition. Kepler-

296 is the most compact system of the multi-planet systems from Table 2, so stability is more sensitive to higher densities.

Finally, we ran long term simulations of the multi-planet systems from Table 4, assuming nominal masses from Lissauer et al. (2011) and nearly circular and coplanar orbits. Nearly all of the candidates from this set have sizes within $2.2\text{--}4.7 R_{\oplus}$, so fall into the super-Earth/sub-Neptune regime, with the exception of one giant planet candidate at $11.2 R_{\oplus}$. All of the systems remained stable for the duration of the simulations.

5. CONCLUSIONS

The *Kepler* mission has provided an enormous amount of data and discoveries that have enabled statistical studies of exoplanets in the terrestrial regime. Although the primary mission duration of *Kepler* was not as long as desired, the duration was sufficient for the orbital period sensitivity to reach into the HZ of the host stars. The primary mission goal of *Kepler* was thus achieved and has provided important insights into the frequency of terrestrial planets in the HZ of late-type stars.

Here we have provided a concise description of HZ boundaries and provide a catalog of *Kepler* candidates that lie in the HZ of their host stars. The four different categories of candidates allow the reader to adopt the criteria that are most useful for a particular follow-up program. For example, giant planets in the optimistic HZ (Table 4) may be useful for those interesting in HZ exomoons where a wider range of incident flux can account for additional energy sources from tidal energy, etc (Heller & Barnes 2013; Hinkel & Kane 2013). Our analysis of the radii distributions for candidates in the HZ compared with the general candidate population shows that the two are very similar within the constraints of selection effects and systematic noise that im-

pacts longer-period terrestrial planets. Our dynamical stability simulations are consistent with all of the multi-planet systems with a planet in the HZ being stable for reasonable assumptions regarding the planet densities and compositions.

Recall that the HZ is primarily a target selection tool rather than any guarantee regarding habitability. Similar catalogs, such as the Catalog of Earth-Like Exoplanet Survey Targets (CELESTA) provided by Chandler et al. (2016) are intended for the design of further missions and observing strategies that will ultimately lead to detailed exoplanet characterization. The utility of catalogs such as the one provided here is to inform the community of the distribution of planetary objects that occupy the HZ and encourage further follow-up and validation of the candidates that remain to be confirmed.

ACKNOWLEDGEMENTS

The authors would like to thank the anonymous referee, whose comments greatly improved the quality of the paper. The authors also thank Douglas Caldwell and Timothy Morton for enlightening discussions regarding *Kepler* candidate validation. Nader Haghighipour acknowledges support from NASA ADAP grant NNX13AF20G. *Kepler* is NASA’s 10th Discovery Mission and was funded by the agency’s Science Mission Directorate. This research has made use of the NASA Exoplanet Archive and the ExoFOP site, which are operated by the California Institute of Technology, under contract with the National Aeronautics and Space Administration under the Exoplanet Exploration Program. This work has also made use of the Habitable Zone Gallery at hzgallery.org. The results reported herein benefited from collaborations and/or information exchange within NASA’s Nexus for Exoplanet System Science (NExSS) research coordination network sponsored by NASA’s Science Mission Directorate.

REFERENCES

Abe, Y., Abe-Ouchi, A., Sleep, N.H., Zahnle, K.J. 2011, *AsBio*, 11, 443

Akeson, R.A., Chen, X., Ciardi, D., et al. 2013, *PASP*, 125, 989

Barclay, T., Quintana, E.V., Adams, F.C., et al. 2015, *ApJ*, 809, 7

Batalha, N.M., Rowe, J.F., Bryson, S.T., et al., 2013, *ApJS*, 204, 24

Bauke, H. 2007, *Eur. Phys. J. B.*, 58 167

Bolmont, E., et al. 2014, *ApJ*, 793, 3

Bolmont, E., Raymond, S.N., Leconte, J., Hersant, F., Correia, A.C.M. 2015, *A&A*, 583, A116

Bolmont, E., Libert, A.-S., Leconte, J., Selsis, F. 2016, *A&A*, in press

Borucki, W.J., Koch, D.G., Basri, G., et al., 2011a, *ApJ*, 728, 117

Borucki, W.J., Koch, D.G., Basri, G., et al., 2011b, *ApJ*, 736, 19

Borucki, W.J., Koch, D.G., Batalha, N., et al., 2012, *ApJ*, 745, 120

Borucki, W.J., Agol, E., Fressin, F., et al. 2013, *Science*, 340, 587

Borucki, W.J. 2016, *Rep on Prog in Physics*, 79, 036901

Burke, C.J., Bryson, S.T., Mullally, F., et al. 2014, *ApJS*, 210, 19

Cartier, K.M.S., Gilliland, R.L., Wright, J.T., Ciardi, D.R. 2015, *ApJ*, 804, 97 M. 2011, *ApJ*, 738, 151

Catanzarite, J., Shao, M. 2011, *ApJ*, 738, 151

Chambers, J.E., 1999, *MNRAS*, 304, 793

Chandler, C.O., McDonald, I., Kane, S.R. 2016, *AJ*, 151, 59

Ciardi, D.R., Beichman, C.A., Horch, E.P., Howell, S.B. 2015, *ApJ*, 805, 16

Coughlin, J.L., Mullally, F.R., Thompson, S.E., et al. 2016, *ApJS*, 224, 12

Désert, J.-M., Charbonneau, D., Torres, G., et al. 2015, *ApJ*, 804, 59

Dressing, C.D., Charbonneau, D. 2013, *ApJ*, 767, 95

Dressing, C.D., Charbonneau, D. 2015, *ApJ*, 807, 45

Forget, F., Pierrehumbert, R.T. 1997, *Science*, 278, 1273

Foreman-Mackey, D., Hogg, D.W., Morton, T.D. 2014, *ApJ*, 795, 64

Fortney, J.J., Marley, M.S., Barnes, J.W. 2007, *ApJ*, 659, 1661

Fressin, F., Torres, G., Charbonneau, D., et al. 2013, *ApJ*, 766, 81

Gaidos, E. 2013, *ApJ*, 770, 90

Gilliland, R.L., Cartier, K.M.S., Adams, E.R., et al. 2015, *AJ*, 149, 24

Gladman, B. 1993, *Icarus*, 106, 247

Hart, M.H. 1978, *Icarus*, 33, 23

Hart, M.H. 1979, *Icarus*, 37, 351

Heller, R., Barnes, R. 2013, *AsBio*, 13, 18

Hinkel, N.R., Kane, S.R. 2013, *ApJ*, 774, 27

Howard, A.W., Marcy, G.W., Bryson, S.T., et al. 2012, *ApJS*, 201, 15

Howard, A.W. 2013, *Science*, 340, 572

Huang, S.-S. 1959, *PASP*, 71, 421

Huang, S.-S. 1960, *PASP*, 72, 489

Jenkins, J.M., Twicken, J.D., Batalha, N.M., et al. 2015, *AJ*, 150, 56

Kaltenegger, L., Haghjipour, N. 2013, *ApJ*, 777, 165

Kane, S.R., Gelino, D.M. 2012a, *PASP*, 124, 323

Kane, S.R., Gelino, D.M. 2012b, *AsBio*, 12, 940

Kane, S.R., Barclay, T., Gelino, D.M. 2013, *ApJ*, 770, L20

Kasting, J.F., Whitmire, D.P., Reynolds, R.T. 1993, *Icarus*, 101, 108

Kasting, J.F., Kopparapu, R., Ramirez, R.M., Harman, C.E. 2014, *PNAS*, 111, 12641

Kitzmann, D., Patzer, A.B.C., Rauer, H. 2013, *A&A*, 557, A6

Kopparapu, R.K., Ramirez, R., Kasting, J.F., et al. 2013, *ApJ*, 765, 131

Kopparapu, R.K., 2013, *ApJ*, 767, L8

Kopparapu, R.K., Ramirez, R.M., SchottelKotte, J., et al. 2014, *ApJ*, 787, L29

Kopparapu, R.K., Wolf, E.T., Haqq-Misra, J., et al. 2016, *ApJ*, 819, 84

Kraus, A.L., Ireland, M.J., Huber, D., Mann, A.W., Dupuy, T.J. 2016, *AJ*, 152, 8

Leconte, J., Forget, F., Charnay, B., Wordsworth, R., Pottier, A. 2013, *Nature*, 504, 268

Leconte, J., Wu, H., Menou, K., Murray, N. 2015, *Science*, 347, 632

Levine, M., Shaklan, S., Traub, W., Kasting, J.F., Dressler, A. 2006, TPF-C Science and Technology Definition Team Final Report, available at http://exep.jpl.nasa.gov/TPF-C/tpf-C_index.cfm

Lissauer, J.J., Ragozzine, D., Fabrycky, D.C., et al. 2011, *ApJS*, 197, 8

Lissauer, J.J., Marcy, G.W., Bryson, S.T., et al., 2014, *ApJ*, 784, 44

Lopez, E.D., Fortney, J.J. 2014, *ApJ*, 792, 1

Mathur, S., Huber, D., Batalha, N., Haas, M.R., Howell, S.B. 2016, Kepler Stellar Properties Catalog Update for Q1-Q17 DR25 Transit Search, available at <http://exoplanetarchive.ipac.caltech.edu/docs/KSCI-19097-001.pdf>

Mischner, M.M., Kasting, J.F., Pavlov, A.A., Freedman, R. 2000, *Icarus*, 145, 546

Morton, T.D., Johnson, J.A. 2011, *ApJ*, 738, 170

Morton, T.D., Swift, J. 2014, *ApJ*, 791, 10

Morton, T.D. 2016, *ApJ*, in press

Mullally, F., Coughlin, J.L., Thompson, S.E., et al. 2015, *ApJS*, 217, 31

Petigura, E.A., Marcy, G.W., Howard, A.W. 2013, *ApJ*, 770, 69

Pierrehumbert, R., Gaidos, E. 2011, *ApJ*, 734, L13

Quintana, E.V., Barclay, T., Raymond, S.N., et al. 2014, *Science*, 344, 277

Rogers, L.A. 2015, *ApJ*, 801, 41

Rowe, J.F., Bryson, S.T., Marcy, G.W., et al. 2014, *ApJ*, 784, 45

Rowe, J.F., Coughlin, J.L., Antoci, V., et al. 2015, *ApJS*, 217, 16

Santerne, A., Díaz, R.F., Moutou, C., et al. 2012, *A&A*, 545, A76

Seager, S. 2013, *Science*, 340, 577

Shields, A.L., Barnes, R., Agol, E., et al. 2016, *AsBio*, 16, 443

Smith, A.W., Lissauer, J.J. 2009, *Icarus*, 201, 381

Stevenson, D.J. 1999, *Nature*, 400, 32

Tenenbaum, P., Jenkins, J.M., Seader, S., et al. 2013, *ApJS*, 206, 5

Toon, O.B., McKay, C.P., Ackerman, T.P., Santhanam, K. 1989, *JGR*, 94, 16287

Torres, G., Kipping, D.M., Fressin, F., et al. 2015, *ApJ*, 800, 99

Traub, W. 2012, *ApJ*, 745, 20

Twicken, J.D., Jenkins, J.M., Seader, S.E., et al. 2016, *ApJ*, submitted (arXiv:1604.06140)

Valencia, D., O'Connell, R.J., Sasselov, D. 2006, *Icarus*, 181, 545

Weiss, L.M., Marcy, G.W. 2014, *ApJ*, 783, L6

Williams, D.M., Pollard, D. 2002, *IJAsB*, 1, 61

Wolf, E., Toon, O.B. 2014, *Geophysical Research Letters*, 41, 167

Wolfgang, A., Lopez, E. 2015, *ApJ*, 806, 183

Wordsworth, R., Pierrehumbert, R. 2013, *Science*, 339, 64

Yang, J., Cowan, N.B., Abbot, D.S. 2013, *ApJ*, 771, L45

Yang, J., Boué, G., Fabrycky, D.C., Abbot, D.S. 2014, *ApJ*, 787, L2

Zsom, A., Seager, S., de Wit, J., Stamenković, V. 2013, *ApJ*, 778, 109